

NJC

Accepted Manuscript



This article can be cited before page numbers have been issued, to do this please use: S. Mabhai, M. Dolai, S. Dey, A. Dhara, B. Das and A. Jana, *New J. Chem.*, 2018, DOI: 10.1039/C8NJ00436F.



This is an Accepted Manuscript, which has been through the Royal Society of Chemistry peer review process and has been accepted for publication.

Accepted Manuscripts are published online shortly after acceptance, before technical editing, formatting and proof reading. Using this free service, authors can make their results available to the community, in citable form, before we publish the edited article. We will replace this Accepted Manuscript with the edited and formatted Advance Article as soon as it is available.

You can find more information about Accepted Manuscripts in the [author guidelines](#).

Please note that technical editing may introduce minor changes to the text and/or graphics, which may alter content. The journal's standard [Terms & Conditions](#) and the ethical guidelines, outlined in our [author and reviewer resource centre](#), still apply. In no event shall the Royal Society of Chemistry be held responsible for any errors or omissions in this Accepted Manuscript or any consequences arising from the use of any information it contains.

A novel chemosensor based on rhodamine and azobenzene moieties for selective detection of Al³⁺ ion

Subhabrata Mabhai,^a Malay Dolai,^b Satyajit Dey,^{*,c} Anamika Dhara,^d Bhriguram Das,^c Atanu Jana,^{*,e}

^aDepartment of Chemistry, Mahishadal Raj College, East Midnapore, Mahishadal, West Bengal, Pin No. 721628, India

^bDepartment of Chemistry, Prabhat Kumar College, Contai, Purba Medinipur 721401, India

^cDepartment of Chemistry, Tamralipta Mahavidyalaya, East Midnapore, West Bengal, Pin No. 721636, India. E-mail: satyajitdeyoc@gmail.com

^dDepartment of Chemistry, Jadavpur University, Raja S. C. Mallick Road, Kolkata 700032, India.

^eDepartment of Chemistry, Indian Institute of Technology, Delhi, HauzKhas, New Delhi-110016, India. E-mail: atanujanaic@gmail.com

Abstract

High absorption coefficient, fluorescence quantum yield, photo stability and relatively long wavelengths of rhodamine dye expand its applicability as a promising fluorescent probe. In the present investigation, two dyes namely rhodamine and azobenzene have been conjugated for the detection of Al³⁺ in aqueous ethanol. The turn on fluorescence response of chemosensor **L** towards Al³⁺ is attributed to the inhibited PET (photo-induced electron transfer) and CHEF (chelation enhanced fluorescence) process along with spiro lactam (non-fluorescent) to ring-opened amide (fluorescent) process. The presence of PET and CHEF process was corroborated by time-resolved photoluminescence study and the spiro lactam ring opening was confirmed by ¹³C NMR and infrared spectroscopy. In presence of Al³⁺, the opened spiro lactam ring forms a 1:1 binding complex with metal which is supported by its high binding constant ($K_a = 7.033 \times 10^3 \text{ M}^{-1}$). Limit of detection (LOD) and limit of quantification (LOQ) value are found to be $1.1 \times 10^{-7} \text{ M}$ and $3.6 \times 10^{-7} \text{ M}$, respectively. The reversible recognition of Al³⁺ was also proved in presence of Na₂EDTA by both UV-Vis and fluorometric titration. The sensing behaviour of chemosensor towards Al³⁺ was supported by DFT/TDDFT calculations.

Keywords: Al sensor, CHEF, Chemosensor, Quantum yield.

Introduction

Malabsorption of Aluminium inhibits several biological activities such as enzyme activity and protein synthesis, alterations in nucleic acid function, and changes in cell membrane permeability. When taken in unregulated amount it causes to osteomalacia,

Parkinson's, Alzheimer's and dialysis diseases.¹⁻⁵ In order to monitor *in vitro* and *in vivo* levels harmful effect in sub-milli and micro molar concentration in environmental, clinical and biological purposes developing of effective Al^{3+} sensor is become crucial. Development of appropriate fluorescent probe for detection of Al^{3+} compared to other transition metal ions encounters some severe problems due to its poor coordination ability, strong hydration ability and lack of spectroscopic characteristics.⁶⁻¹¹ To overcome these problems, some serious efforts has been made for the development of aluminium sensing fluorescent probes such as BINOL,¹² BODIPY,¹³ 8-hydroxyquinoline,¹⁴ anthraquinone,¹⁵ coumarin,⁹ Schiff base molecules.¹⁶⁻¹⁹ Majority of these probes provide moderate success because of difficult synthetic methodologies,¹³ limited solubility, poor selectivity and interfering sensitivity towards other d-block cations like Fe^{3+} and Zn^{2+} . Hence, invention of new superior effective probe for Al^{3+} is still demanding. Spirocyclic Rhodamine derivatives have wide applications as chemodosimeter due to their unique photo physical properties.²⁰⁻²⁴ Rhodamine derivatives exhibit some unique fluorescence "OFF-ON" behavior through change in architecture from color less spiro lactam ring to intense pink colored ring opened amide system in the presence of analyte.

Herein, we report the design, synthesis and photophysical properties of a new 2-Hydroxy-5-(4-nitrophenyl)diazenyl) benzaldehyde-appended rhodamine based scaffold (**L**) as a chemosensor, which showed strong reversibility, sensitivity and selectivity towards Al^{3+} in a mixed solvent through binding induced changes in the electronic spectral pattern via the chelation enhanced fluorescence (CHEF) process²⁵⁻²⁸ and spiro lactam ring opening phenomena. The sensing mechanism has also been corroborated by DFT calculations.

Experimental

Materials

Rhodamine B (99.0%), Salicylaldehyde (98%), p-nitro aniline (97%) and all other analytical grade materials (metal salts and solvents) were purchased from Sigma-Aldrich and were used without further purification. Any spectral change of the chemosensor moiety was recorded in a constant ligand concentration with the addition of metal perchlorate salts. Metal perchlorate salts were prepared according to literature method.²⁹ Stock solution for chemosensor **L** was prepared in EtOH-H₂O (4:1, v/v) pH = 7.2 using 20 μM HEPES buffer at 25 °C. Distilled water was used throughout the experiment.

Physical measurements

The fluorescence spectra and relative fluorescence intensity were recorded using a XENO Flash (PTI) fluorescence spectrophotometer with excitation wavelength at 500 nm for both ligand and complex. An Evolution-201 spectrometer was used for absorption measurements. IR spectra (KBr pellet, 400–4000 cm^{-1}) were recorded on a Perkin-Elmer infrared spectrophotometer (Model: 883). The ^1H NMR spectra were performed on Bruker 400 MHz instrument in CDCl_3 using TMS as internal standard. Chemical shifts δ were reported in ppm unit and ^1H - ^1H coupling constants in Hz. Mass spectra were recorded on Qtof Micro YA263 mass spectrometer. Elemental analysis (C, H, N) result was obtained from Perkin Elmer 2400 CHN analyser. DFT calculations have been done using Gaussian software. Fluorescence lifetimes were measured by the method of Time Correlated Single-Photon Counting (TCSPC) using a HORIBA Jobin Yvon Fluorocube-01-NL fluorescence lifetime spectrometer.

Computational method

DFT is an important tool to investigate the geometry, electronic structure, and optical properties. Ground state electronic structure calculations in gas phase of both the ligand and complex have been performed using DFT³⁰ method associated with the conductor-like polarizable continuum model (CPCM).^{31–33} Becke's hybrid function³⁴ with the Lee-Yang-Parr (LYP) correlation function³⁰ was used through the study. The geometries of the ligand and complex were fully optimized without any symmetry constraints. On the basis of the optimized ground state geometry, the absorption spectral properties in methanol (CH_3OH) media were calculated by time-dependent density functional theory (TDDFT)^{35–37} approach associated with the conductor-like polarizable continuum model (CPCM).^{31–33} We computed the lowest 40 singlet – singlet transition and results of the TD calculations were qualitatively very similar. The TDDFT approach had been demonstrated to be reliable for calculating spectra properties of many transition metal complexes.^{38–41} Due to the presence of electronic correlation in the TDDFT (B_3LYP) method it can yield more accurate electronic excitation energies. Hence TDDFT had been shown to provide a reasonable spectral feature for our complex of investigation.

We have run the Gaussian for geometry optimization of both the ligand and the complex in ground state with 6-31G under B_3LYP . For Al atom, we used 6-31G**^{*}; for C, H, N and O atoms we employed 6-31G** as basis set under B_3LYP and compare the results, which didn't not show any significant change in geometrical parameters. All the calculations were done

with the Gaussian 09W software package. GaussSum 2.1 program⁴² was used to calculate the molecular orbital contributions from groups or atoms.

Synthesis of 2-Hydroxy-5-(4-nitrophenyl) diazenyl benzaldehyde:

The compound was prepared according to literature method (Fig. S1, ESI).^{43,44} The p-nitro aniline (0.57 g, 4.12 mmol) was dissolved in 2 mL concentrated hydrochloric acid to obtain a clear green solution. Temperature of the beaker was kept in between 0 °C – 5 °C by placing it on an ice-salt bath while the solution was stirred vigorously. A cold solution of NaNO₂ was prepared by dissolving (0.284 g, 4.12 mmol) sodium nitrite in 1 ml water which was added to the green solution drop wise slowly with constant stirring. This time colour of the solution changed from green to pale yellow. The pale yellow diazo solution was added at 5 °C to a solution of salicylaldehyde (0.503 g, 4.12 mmol) in 20 ml H₂O which contained NaOH (0.165 g, 4.12 mmol) and Na₂CO₃ (0.266 g, 2.51 mmol). The resulting solution was stirred overnight at room temperature. The dark brown cake was then filtered by using whatman-41, filtrate was discarded, and the dark-brown residue was washed repeatedly with 10 % NaCl solution. Solid residue was taken in a beaker and reslurried by adding water. Nearly 2-3 drops of concentrated HCl was added to it to maintain the pH at 4-5. Finally the orange colour product was kept in vacuum for drying and was chromatographed for confirmation. The yield of the product was 80 %. M.P. 180 °C.

¹H NMR (CDCl₃, 400 MHz): δ 11.4 (s, 1H, Ar-OH), 10.06 (s, 1H, Ar-CHO), 8.41-8.39 (d, 2H, J = 8 Hz, Ar-H), 8.31 (s, 1H, Ar-H), 8.22 - 8.21 (d, 1H, J = 4 Hz, Ar-H), 8.04-8.02 (d, 2H, J = 8 Hz, Ar-H), 7.18-7.16 (d, 2H, J = 8 Hz, Ar-H). (Fig. S1, ESI)

Synthesis of Rhodamine B hydrazide:

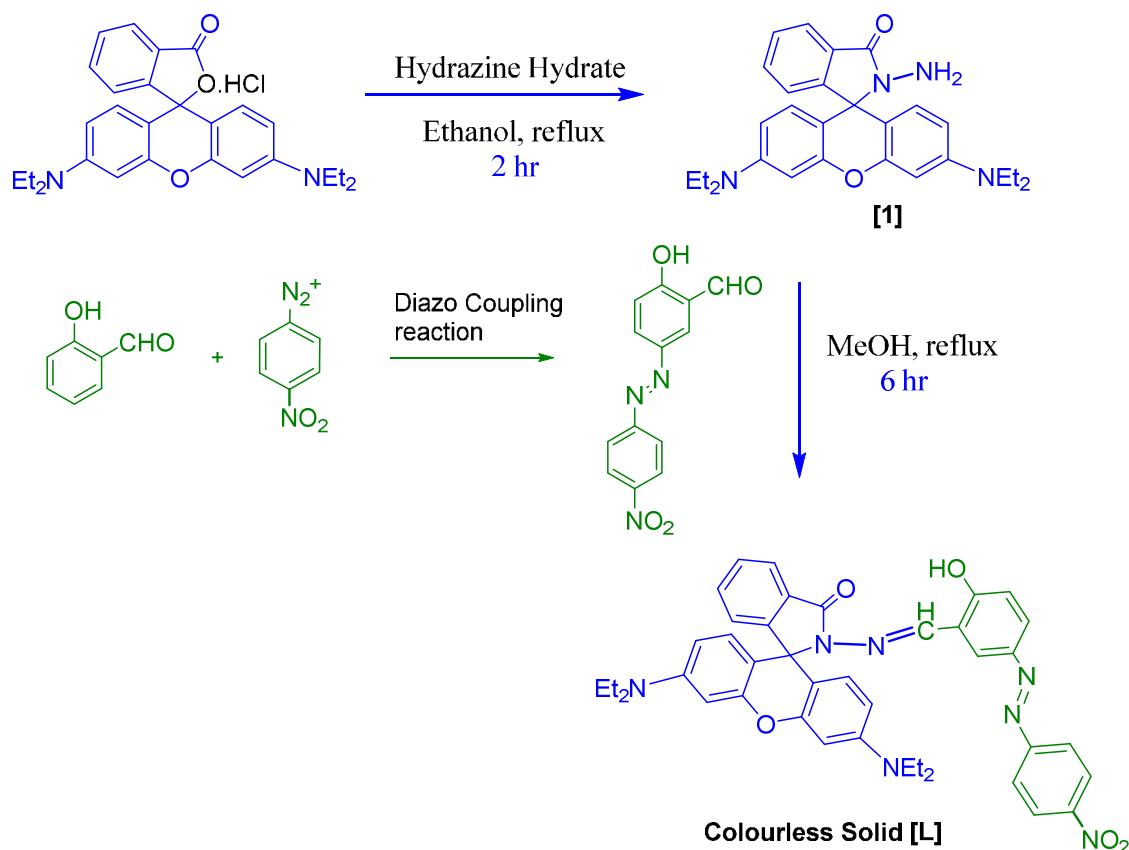
Rhodamine B hydrazide was synthesized according to reported method.⁴⁵

Synthesis of chemosensor L

The synthesis of chemosensor **L** was done by the condensation reaction of aldehyde precursor with Rhodamine B hydrazide under refluxing condition [Scheme 1]. In this process Rhodamine B hydrazide (0.536 g, 1.175 mmol) and 2-Hydroxy-5-(4-nitrophenyl) diazenyl benzaldehyde (0.317 g, 1.175 mmol) was taken in 20 ml ethanol and refluxed with CaCl₂ guard tube at the top of the condenser. Progress of the reaction was monitored with TLC and after nearly 4 hours of refluxing a maroon coloured solid was appeared which was cooled to room temperature. The final volume of the suspended solution was reduced 1/3 of the total volume by heating in water bath. The yellowish precipitate was obtained by normal

gravimetric filtration and repeated washing with cold EtOH-Ether (1:1 ratio). Yield ~ 65 %. M.P. 260 °C.

^1H NMR [400 MHz, CDCl_3 , δ (ppm)] : 11.65 (s, 1H, Ar-OH (H-bonded)), 9.21 (s, 1H, Ar-CH=N-), 8.36-8.34 (d, 2H, , J = 9 Hz Ar-H), 8.00-7.93 (m, 3H, Ar-H), 7.87-7.80 (m, 2H, Ar-H), 7.57-7.53 (m, 2H, Ar-H), 7.20-7.19 (d, 1H, J = 6.4 Hz, Ar-H), 7.01-6.99 ((d, 1H, J = 8.4 Hz, Ar-H), 6.52-6.50 (m, 4H, Xanthene-H, J = 8 Hz), 6.29-6.27 (d, 2H, Xanthene-H, J = 8 Hz), 3.34-3.32 (d, 8H, N-CH₂-CH₃, J = 6.4 Hz), 1.16-1.19 (t, 12H, N-CH₂-CH₃, J = 6.4 Hz), (**Fig. S2, ESI**). ^{13}C NMR [800 MHz CDCl_3 , δ (ppm)] : 12.62, 44.38, 66.45, 97.94, 105, 108.18, 118.23, 118.93, 123.12, 123.52, 124.24, 124.75, 125.49, 128.11, 128.49, 128.75, 129.47, 135.85, 145.55, 148.22, 149.18, 150.77, 150.9, 153.53, 156, 162.8, 164.51. (**Fig. S3, ESI**). CHN Analysis for $\text{C}_{41}\text{H}_{39}\text{N}_7\text{O}_5$: calculated (%): C, 69.38; H, 5.54; N, 13.81; O, 11.27; Found (%): C, 69.35; H, 5.56; N, 13.83; O, 11.25. ESI-MS: m/z calculated for $\text{C}_{41}\text{H}_{39}\text{N}_7\text{O}_5$ $[\text{M}+\text{H}]^+$: 710.30, found 710.30 (100 %). (**Fig. S4, ESI**)



Scheme 1. Synthesis of chemosensor L

Synthesis of L-Al³⁺ complex

Al(NO₃)₃·9H₂O (0.19 g, 0.506 mmol) was added to a stirring solution of ligand (0.359 g, 0.506 mmol) in CH₃CN and stirred overnight at room temperature. Solution was filtered and filtrate kept one week for slow evaporation. The deep maroon solid appeared was collected and vacuum dried after several time washing with methanol. ESI-MS: m/z calculated for C₄₁H₃₉N₇O₅ [L+Al+H₂O+H⁺]⁺ : 756.28, found 756.2885 (100 %) (**Fig.S5, ESI**).

Association constant

The association constant for the formation of the complex, [L-Al³⁺] were determined using the Benesi–Hildebrand (B–H) equation.⁴⁶

$$\frac{1}{(A - A_0)} = \frac{1}{[K(A_{\max} - A_0)C]} + \frac{1}{(A_{\max} - A_0)}$$

where A₀ is the absorbance maxima of sensor L, A is the observed absorbance at that particular wavelength at different concentration of the metal ion (C), A_{max} is the maximum absorbance value at λ_{max} = 554 nm (for Mⁿ⁺) during titration with varying [C], K is the association constant and was determined from the ratio of slope and intercept of the linear plot, and [C] is the concentration of the Mⁿ⁺ ion added during titration studies. The goodness of the linear fit of the B–H plot of 1/(A-A₀) vs. 1/[Mⁿ⁺] for 1:1 complex formation confirms the binding stoichiometry between sensor and Mⁿ⁺.

(b)The binding constant for sensor L–Metal complex was also determined using the Benesi–Hildebrand relation from **spectrofluometric** titration.

$$\frac{1}{(I - I_0)} = \frac{1}{(I_1 - I_0)} + \frac{1}{(I_1 - I_0)k[M^{n+}]^m}$$

where [Mⁿ⁺] is the metal ion concentration, I₀, I and I₁ indicate emission intensities in the absence of, at intermediate and at infinite concentrations of metal ions, respectively. For 1:1 complexation, m = 1 and for 1:2 complexation, m = 2.

Procedure for metal ion sensing

For both UV-Vis and fluorescence spectral study titration was carried out by taking 2.5 mL solution of ligand (40 μM) and (100 μM) metal ions solution in a quartz cuvette (path

length, 100 cm). Before recording the UV-Vis spectra the resulting solution was incubated for 30 min after shaking. The excitation wave length was 500 nm.

Fluorescence Quantum Yield

Fluorescence quantum yield of the sensor was determined in spectroscopic grade methanol using Fluorescein as an optically matching reference with a known Φ_r (0.79) according to the following equation.

$$\Phi_s = \Phi_r \left(\frac{A_r F_s}{A_s F_r} \right) \left(\frac{\eta_s^2}{\eta_r^2} \right)$$

where A_s and A_r are the absorbance of the sample and reference solutions, respectively, at the same excitation wavelength, F_s and F_r are the corresponding relative integrated fluorescence intensities, and η is the refractive index of the solvents. We measured the quantum yield of our sensor in presence and absence of Al^{3+} , and our experimental results revealed that the bare sensor has the quantum yield, $\Phi = 0.51\%$, and that of **L**- Al^{3+} complex is 4.08 % which is almost 8 times higher than bare sensor.

Result and Discussion:

UV-Visible spectroscopic studies:

The sensing behaviour of the sensor **L** was investigated by monitoring its UV-Visible and fluorescence spectra in the presence of different metal ions in EtOH-H₂O (4:1, v/v) pH = 7.2 using 20 μM HEPES buffer at 25 °C. Initially the sensing ability of the sensor **L** was examined by recording the UV-Visible absorption spectra by adding 100 μM stock solutions of several metal ions including Ba^{2+} , Ca^{2+} , Cd^{2+} , Cr^{3+} , Cu^{2+} , Fe^{3+} , Fe^{2+} , Hg^{2+} , K^+ , Mg^{2+} , Mn^{2+} , Na^+ , Ni^{2+} , Pb^{2+} , and Al^{3+} to 40 μM sensor solution taken in quartz tube containing 2 mL EtOH-H₂O (4:1, v/v) pH = 7.2 using 20 μM HEPES buffer at 25 °C. As shown in the **Fig. 1**, it is interesting to note that except Al^{3+} and Cu^{2+} ions no other metal cations altered the UV-Visible spectral nature of the sensor **L**. Addition of Al^{3+} and Cu^{2+} to sensor **L** resulted in the appearance of strong bands at $\lambda_{\text{max}} = 554$ & 550 nm, respectively, in the visible region of the absorption spectrum of **L** associated with immediate changes of colourless sensor solutions to deep pink colour which was clearly visible to naked eye for direct recognition [**Fig. 2a**]. Appearance of these new absorption spectral bands in the visible region of the UV-Visible spectrum demonstrated that the conjugated xantheno framework was generated by opening of the spirolactam ring due to the complex formation by metal ion chelation.

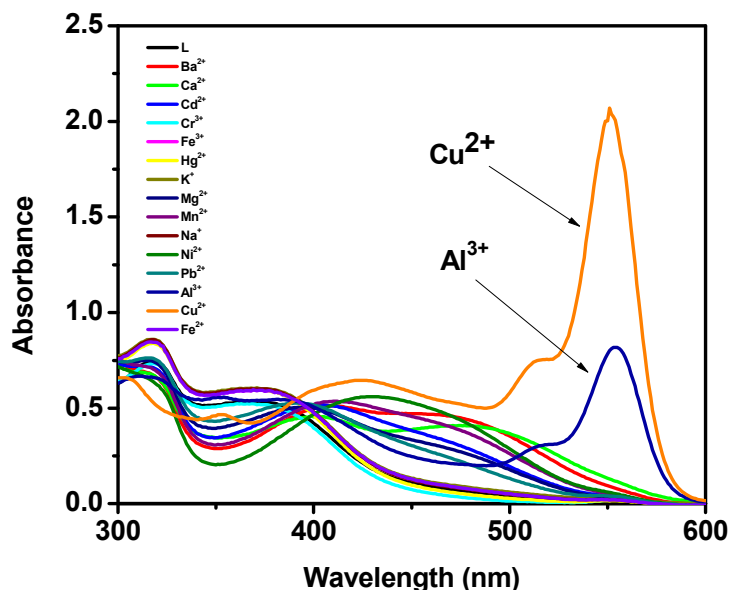


Fig. 1: UV-Vis spectral nature of **L** (40 μM) upon addition of various metal ions (Ba^{2+} , Ca^{2+} , Cd^{2+} , Cr^{3+} , Fe^{3+} , Fe^{2+} , Hg^{2+} , K^+ , Mg^{2+} , Mn^{2+} , Na^+ , Ni^{2+} , Pb^{2+} , Al^{3+} and Cu^{2+}), in a HEPES buffer [50 μM , $\text{C}_2\text{H}_5\text{OH-H}_2\text{O}$ (4:1,v/v) pH = 7.2] at 25 $^\circ\text{C}$.

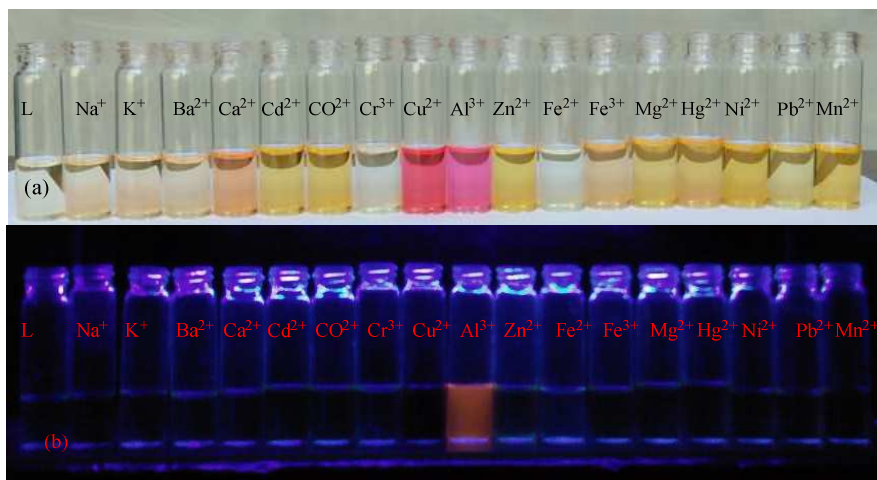


Fig. 2: Visual display of **L** plus metal ions: (a) naked eye (b) under UV cabinet.

UV-Visible titrations of the sensor **L** with Al^{3+} and the resulting **L-Al**³⁺ complex with Na_2EDTA were carried out to check the reversible binding nature of the sensor. As depicted in **Fig. 3**, it was clearly observed that gradual incremental Al^{3+} additions (0-110 μM) to sensor **L** (40 μM) in $\text{EtOH-H}_2\text{O}$ (4:1, v/v) pH = 7.2 using 20 μM HEPES buffer at 25 $^\circ\text{C}$ resulted in gradual enhancement of the absorption intensity of the absorption band at $\lambda_{\text{max}} = 554 \text{ nm}$ along with the development and deepening of the pink colour. However, the incremental addition of a strong chelating agent, Na_2EDTA (0-435 μM), to the resulting **L-**

Al^{3+} complex solution showed immediate decrease in intensity of the above absorption band [Fig. 4] with disappearance of the pink colour. This was due to the regeneration of free sensor by demetallation of Al^{3+} from the L-Al^{3+} complex indicating the reversible binding nature of the sensor. Similarly UV-Visible titrations of the sensor **L** with Cu^{2+} and the resulting L-Cu^{2+} complex with Na_2EDTA were carried out to check the binding nature and reversibility of the sensor (Fig. S6, S7, ESI). Maximum absorbance of **L** was observed upon incremental addition of $20\ \mu\text{M}$ Cu^{2+} due to strong (1:1) binding nature of **L** with Cu^{2+} which was further proved from Job's plot experiment (Fig. S8 ESI).⁴⁷ The binding constant for Cu^{2+} was calculated from B-H equation to be $1.45 \times 10^4\ \text{M}^{-1}$ (Fig. S9 ESI).

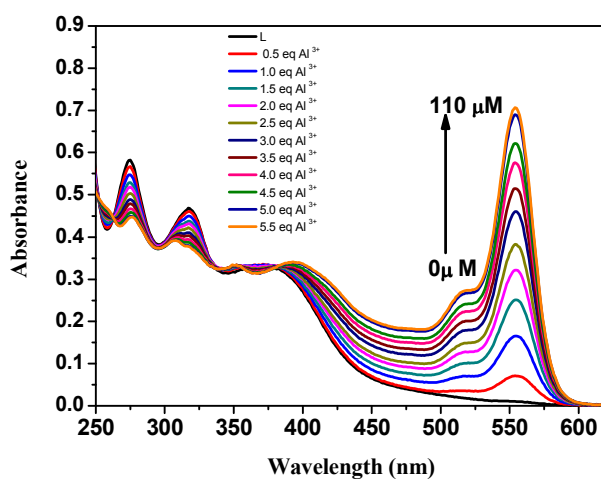


Fig. 3: UV-Vis spectral changes of **L** ($40\ \mu\text{M}$) upon addition of Al^{3+} ions in a HEPES buffer [$50\ \mu\text{M}$, $\text{C}_2\text{H}_5\text{OH-H}_2\text{O}$ (4:1, v/v, pH= 7.2)] at $25\ ^\circ\text{C}$. [Al^{3+}] = 0-110 μM .

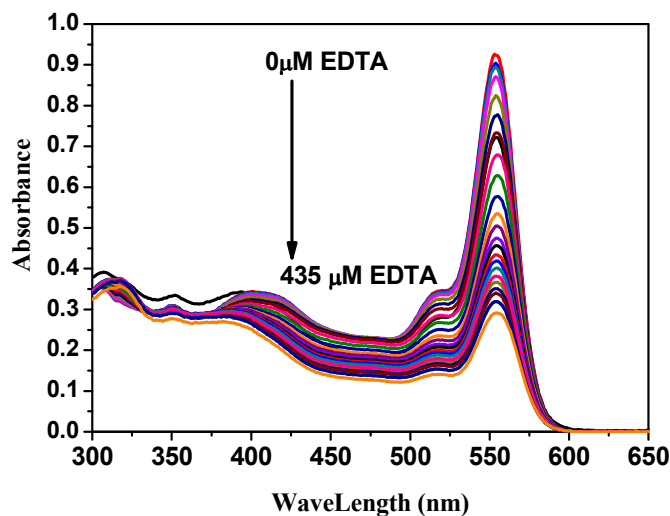


Fig. 4: UV-Vis spectral changes of Al^{3+} complex of **L** ($40\ \mu\text{M}$) upon addition of EDTA in a HEPES buffer [$50\ \mu\text{M}$, $\text{C}_2\text{H}_5\text{OH-H}_2\text{O}$ (4:1, v/v, pH= 7.2)] at $25\ ^\circ\text{C}$. EDTA added = 0-435 μM

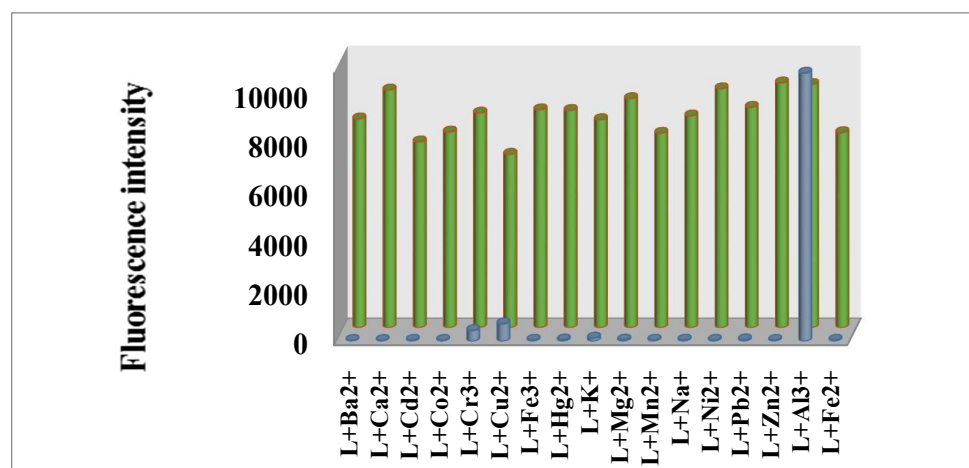


Fig. 5: Fluorescence intensity of **L** (40 μM) in the presence of various metal cations in a HEPES buffer [50 μM , $\text{C}_2\text{H}_5\text{OH}-\text{H}_2\text{O}$ (4:1, (v/v), pH 7.2] at 25 $^\circ\text{C}$. The blue bars represent the fluorescence intensities of sensor **L** in the presence of metal cations of interest. The green bars represent the change of fluorescence intensity that occurred upon subsequent addition of Al^{3+} ion to the above mentioned solution. $\lambda_{\text{ex}} = 500 \text{ nm}$

In order to investigate the recognizing ability of **L** towards Al^{3+} in the presence of other competing metal cations, we subsequently recorded UV-Visible spectra of the sensor **L** in the presence of Al^{3+} (100 μM) mixed with other competing metal cations (100 μM) such as Ba^{2+} , Ca^{2+} , Cd^{2+} , Co^{2+} , Cr^{3+} , Cu^{2+} , Fe^{3+} , Fe^{2+} , Hg^{2+} , K^+ , Mg^{2+} , Mn^{2+} , Na^+ , Ni^{2+} , Pb^{2+} , Zn^{2+} and Al^{3+} as shown in **Fig. 5**, we found that the absorbance intensity and band position of the **L**- Al^{3+} complex remained unaltered in the presence of different metal cations. This observation strongly supports that the selectivity of this Al^{3+} sensor is not affected by the presence of other metal ions.

Furthermore, in order to get deeper inside into the binding behaviour of the sensor **L** with Al^{3+} , the Job's plot using UV-Visible titrations of the sensor **L** and Al^{3+} with a total concentration of 20 μM was utilized. Analysis of the Job's plot showed that highest UV-Visible absorption occurred at 0.5 mole fraction of Al^{3+} implying the 1:1 stoichiometry of the **L**- Al^{3+} complex (**Fig. S13, ESI**). Further evidence for 1:1 stoichiometric complexation between the sensor **L** and Al^{3+} was obtained from ESI-MS spectrum of the complex (**Fig. S5, ESI**) which exhibited a peak at m/z 755.286 for $[\text{L}+\text{Al}^{3+}+\text{H}_2\text{O}]^+$. Based on the 1:1 binding stoichiometry, Benesi-Hildebrand plot of the UV-Visible titration data provided a linear curve and the association constant (k_a) was calculated to be $7.033 \times 10^3 \text{ M}^{-1}$ (**Fig. S14, ESI**). The detection limit was also calculated by 3σ method⁴⁸ and found to be $1.1 \times 10^{-7} \text{ M}$. in

EtOH-H₂O(4:1, v/v) pH = 7.2 using 20 μM HEPES buffer at 25 °C (**Fig. S15, ESI**). The potentiality for any chemosensor to be used successfully lies on its lower detection limit. The limit of detection value of our sensor is much lower as compared to others (**Table S1, ESI**), and hence it has a stronger potentiality to be used as environment friendly chemosensor.

Fluorescence spectroscopic studies

The sensing behaviour of the sensor **L** was also pursued by fluorescence spectroscopic studies. The experimental results revealed that upon excitation at $\lambda_{\text{ex}} = 500$ nm, the sensor **L** itself and in the presence of different metal ions such as Ba²⁺, Ca²⁺, Cd²⁺, Co²⁺, Fe³⁺, Fe²⁺, Hg²⁺, K⁺, Mg²⁺, Mn²⁺, Na⁺, Ni²⁺, Pb²⁺, Zn²⁺ and Al³⁺ in EtOH-H₂O (4:1, v/v), pH = 7.2 using 20 μM HEPES buffer at 25 °C displayed no noticeable emission band above $\lambda_{\text{max}} = 500$ nm. Addition of Cr³⁺ and Cu²⁺ to the sensor solution showed very weak emission band at $\lambda_{\text{max}} = 578$ & 580 nm, respectively. However, in the presence of Al³⁺, a remarkable enhancement of fluorescence intensity was observed at $\lambda_{\text{max}} = 582$ nm [**Fig. 6a and 6b**] due to the happening of CHEF as well as inhibited PET process. The lone pair (lp) from -NEt₂ group can move to azobenzene moiety causing **L** as non-fluorescent molecule. But, this lp in **L** is unavailable upon binding with Al³⁺ ion in Al³⁺-complex making the **L** as fluorescent where PET process is inhibited. This strong affinity towards Al³⁺ can be attributed by the fact that trivalent Al have stronger binding energy (nearly double) to **L** than Cu²⁺, and hence it displaces Cu²⁺ almost completely making the **L** highly selective for Al³⁺.⁴⁹ Al³⁺ possesses a high charge and small ionic radius, and consequently, it bears a high ionic potential value making it a hard acid. So the ligand (**L**) having binding site with N and O has a strong tendency for chelation with Al³⁺ following the well-known SHAB (hard and soft acids and bases) principle and hence sensor containing N and O as donor site is very common for Al³⁺.⁵⁰⁻⁵² Ba²⁺, Ca²⁺ and Cu²⁺ are hard acids and hence according to SHAB principle they can bind with the hard base centres like N and O exhibiting color change under visible light. It is noteworthy that Cu²⁺, a d⁹ system being paramagnetic showed strong fluorescence quenching phenomena upon binding with **L**.⁵³ Though Ca²⁺, Ba²⁺ and Al³⁺ are p-block elements, the stabilisation energy of L-Al³⁺ is much higher than the L-Ba²⁺ and L-Ca²⁺ complexes. Consequently, L-Al³⁺ complex exhibited prominent color under UV light.⁴⁹

Furthermore, under UV lamp of long wave length (360 nm), addition of 2.5 equivalents of Al³⁺ to the sensor solution showed a prominent colour change from colourless to an intense orange fluorescence, demonstrating Al³⁺ selective "turn-on" fluorescence signalling behaviour of **L** [**Fig. 2b**]. The reversible behaviour of **L** was also examined by

fluorimetric titration method. The experimental observation revealed that upon gradual incremental addition of Al^{3+} to the sensor solution resulted in the gradual enhancement of emission intensity of the emission band around $\lambda_{\text{max}} = 582 \text{ nm}$ in the emission spectrum of the sensor **L**, which was gradually decreased on successive excess of Na_2EDTA addition [**Fig. 7 and 8**]. These observations once again confirmed that our sensor can definitely be utilized as a selective fluorescent "on-off" sensor for Al^{3+} .

We have confirmed our proposed mechanism of **L**- Al^{3+} complex formation through comparison of both IR and ^{13}C NMR spectrum of free sensor (**L**) and **L**- Al^{3+} Complex. The carbonyl stretching frequency of spirolactam ring in free sensor and the **L**- Al^{3+} complex are 1725 cm^{-1} and 1647.5 cm^{-1} , respectively. This shifting (77.5 cm^{-1}) indicates the spirolactam ring opening phenomena where carbonyl oxygen make a bond towards Al^{3+} ion as reported earlier (**Fig. S10 and S11, ESI**).^{54,55} The spirolactam ring opening mechanism was also established from the disappearance of the tertiary carbon signal appeared at $\delta = 66.45 \text{ ppm}$ and appearance of a new signal at $\delta = 134.28 \text{ ppm}$ upon addition of Al^{3+} (**Fig. S12, ESI**).^{56,57} This is attributed to the conversion of sp^3 spiro carbon of rhodamine to sp^2 carbon upon binding with Al^{3+} ion.

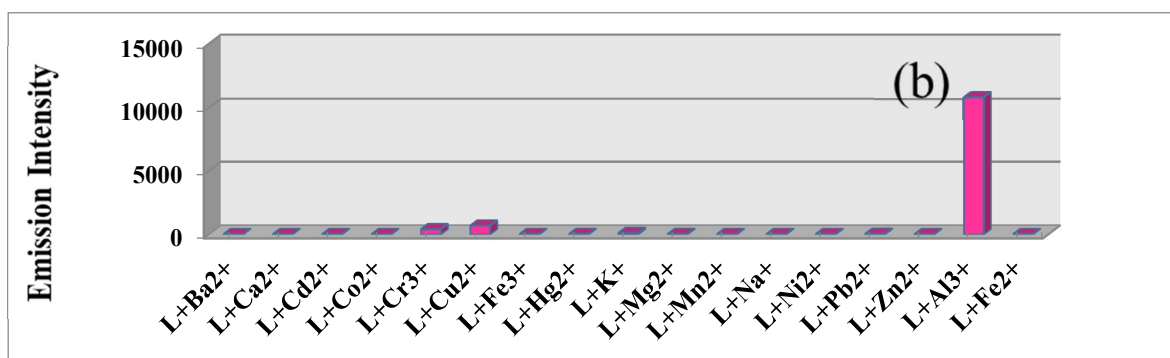
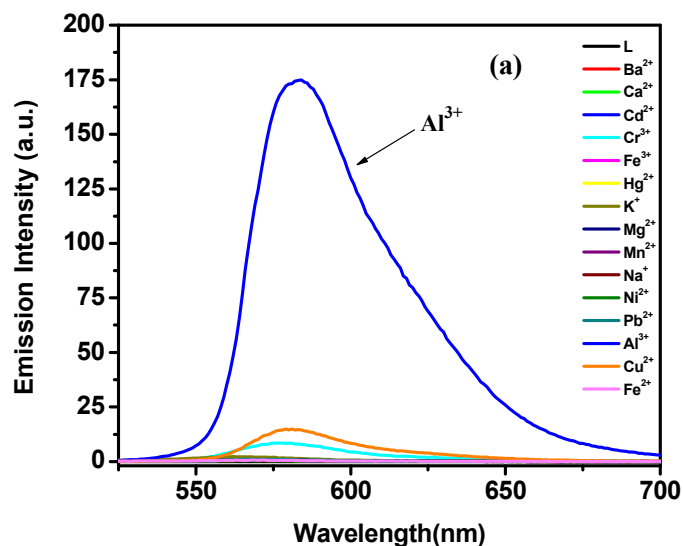


Fig. 6: (a) Emission spectral nature of L (40 μM) upon addition of various metal ions (Ba^{2+} , Ca^{2+} , Cd^{2+} , Co^{2+} , Cr^{3+} , Cu^{2+} , Fe^{3+} , Fe^{2+} , Hg^{2+} , K^+ , Mg^{2+} , Mn^{2+} , Na^+ , Ni^{2+} , Pb^{2+} , Zn^{2+} , Al^{3+}) in a HEPES buffer [50 μM , $\text{C}_2\text{H}_5\text{OH}-\text{H}_2\text{O}$ (4:1,v/v, pH= 7.2)] at 25 $^\circ\text{C}$ (b) Column plot for the emission spectral intensity of L (50 μM) upon addition of different metal ions (Ba^{2+} , Ca^{2+} , Cd^{2+} , Cr^{3+} , Cu^{2+} , Fe^{3+} , Fe^{2+} , Hg^{2+} , K^+ , Mg^{2+} , Mn^{2+} , Na^+ , Ni^{2+} , Pb^{2+} , and Al^{3+}) in a HEPES buffer [50 μM , $\text{C}_2\text{H}_5\text{OH}-\text{H}_2\text{O}$ = (4:1,v/v, pH= 7.2)] at 25 $^\circ\text{C}$.

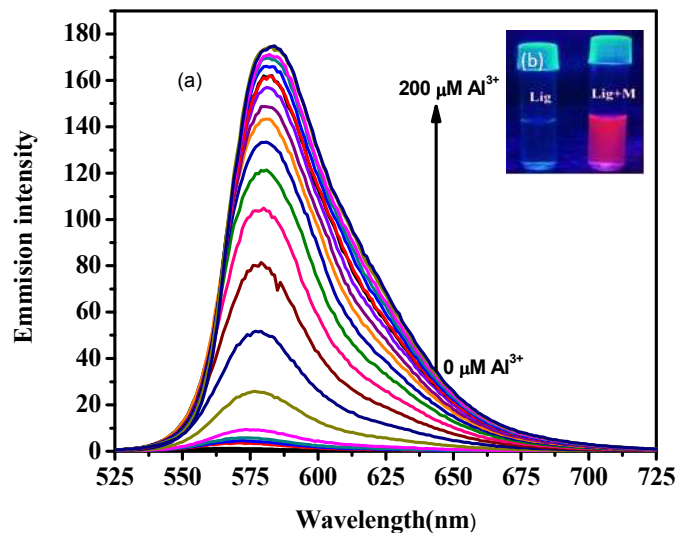


Fig. 7: (a) Emission spectral changes of L (40 μM) upon addition of Al^{3+} ion in a HEPES buffer [50 μM , $\text{C}_2\text{H}_5\text{OH-H}_2\text{O}$ (4:1, v/v, pH= 7.2)] at 25 $^\circ\text{C}$. [Al^{3+}] = 0-200 μM (b) only L and L in presence of Al^{3+} ion under UV light.

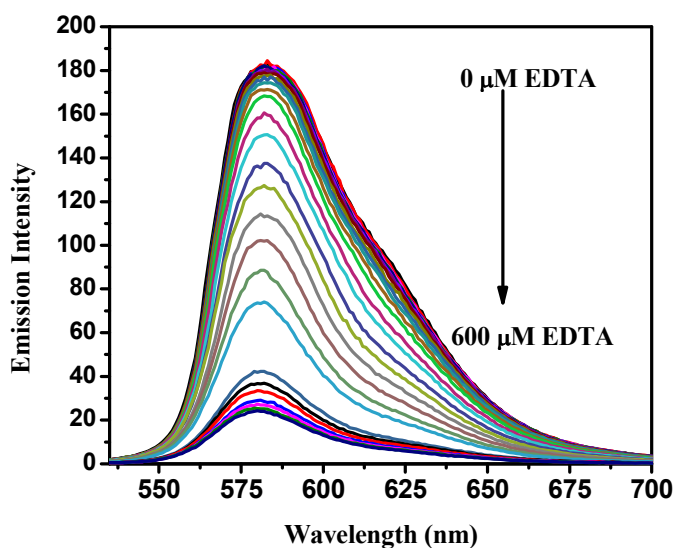
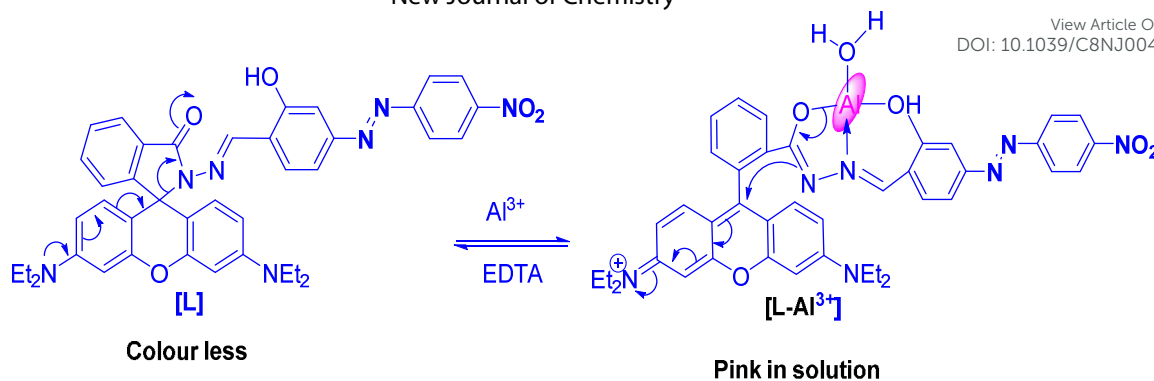


Fig. 8: Emission spectral changes of Al^{3+} complex of L (40 μM) upon addition of EDTA in a HEPES buffer [50 μM , $\text{C}_2\text{H}_5\text{OH-H}_2\text{O}$ (4:1, v/v, pH= 7.2)] at 25 $^\circ\text{C}$. EDTA = 0-600 μM



Scheme 2. Probable binding mode of chemosensor **L** with Al^{3+}

Effect of pH

To explore our sensor **L** as an effective tool for detecting Al^{3+} ion in physiological pH, we evaluated the sensitivity of **L** in the absence and presence of Al^{3+} ion in different acidic and basic pH values. As shown in **Fig. 9**, in the absence of Al^{3+} , no characteristic change in the fluorescence spectra of the sensor was recorded between pH 4.0 and 8.0, which indicates that **L** must remain in the spirocyclic form within this pH range. In presence of Al^{3+} , the spectral responses of the sensor remained almost steady without any interference by proton between the pH 4.0 and 8.0. At pH lower than 4.0, the fluorescence intensity of the sensor increased gradually in the absence and presence of analyte due to the generation of ring opening xanthenone moiety by protonation of the amide carbonyl.^{58,59} At basic pH i.e.; pH > 8, the emission intensity of the **L-Al³⁺** complex decreased slowly due to the generation of free ligand by the removal of Al^{3+} ion as its oxide. As the spectral responses of the sensor as well as sensor plus Al^{3+} remained almost unchanged within a broad pH range which covered the physiological pH (7.2), so the sensor can be used for the detection of Al^{3+} ion in physiological conditions.

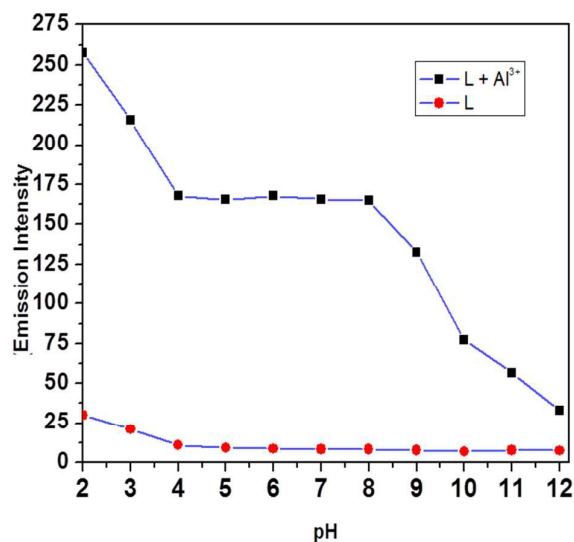


Fig. 9: Effect of pH in absence and in presence of Al³⁺ ion [50 μ M C₂H₅OH-H₂O (4:1,v/v, pH=7.2)] at 25 °C and at excitation wave length = 500 nm and emission wavelength = 582 nm

Geometry optimization and electronic structure.

The optimized geometry of L and its Al (III) complex is shown in [Fig. 10]. The ground state geometry optimization for the ligand (L) and complex **1** were performed in gas phase. Main optimized geometrical parameters of the complex **1** are listed in [Table 1]. The geometry of the penta-coordinated metal center can be measured by the Addison parameter (τ), which is 0.114 for **1** in this case [$\tau = (\alpha - \beta)/60$, where α and β are the two largest Ligand-Metal-Ligand angles of the coordination sphere], suggesting a distorted square pyramidal geometry of around the Al (III) center ($\tau = 0$ for a perfect square pyramid and $\tau = 1$ for a perfect trigonal bi-pyramidal). In **1**, all calculated Al-N distances occur in the range 1.968 Å and Al-O distances are in the range 1.795-1.919 Å. On complexation, some C-N and C-O bond lengths are changed with respect to that in free ligand and [Table 2] describes the change in bond lengths in **1** compared to free ligand L.

In case of HL at ground state, the electron density at HOMO-2, LUMO, LUMO+1 and LUMO+2 orbitals are mainly reside on the benzene moiety while a considerable contribution comes from p-nitro azo-benzene moiety along with the contribution of rhodamine moiety in HOMO-3, HOMO-1 and HOMO orbitals. The energy difference between HOMO and LUMO is 2.08 eV of ligand (L). In case of **1**, all the HOMO, HOMO-1 and HOMO-5 orbitals are mainly originating from ligand π and π^* orbital contribution while the HOMO-2,

LUMO and LUMO+1 orbitals arises from metal *d* orbital contribution along with ligand π orbital contribution. The energy difference between HOMO and LUMO is 2.69 eV of **1**. These compositions are useful in understanding the nature of transition as well as the absorption spectra of both the ligand and complex (vide infra). The ligand shows two absorption band at 385 nm in methanol solution at room temperature. This assignment was supported by TDDFT calculations. This absorption band can be assigned to the $S_0 \rightarrow S_{14}$ transition. The absorption energies along with their oscillator strengths, the main configurations and their assignments calculated using TDDFT method using the ground state geometry for HL is discussed here and the related data are given in [Table 3]. The complex shows three absorption bands at 553, 514 and 400 nm in methanol solution at room temperature. The TDDFT calculated absorption bands are located at 545, 513 and 399 nm for **1**, which are in good agreement with experimental results of 553, 514 and 400 nm [Table 4]. These three absorption bands can be assigned to the $S_0 \rightarrow S_2$, $S_0 \rightarrow S_3$ and $S_0 \rightarrow S_{11}$ transitions, respectively [Table 4].

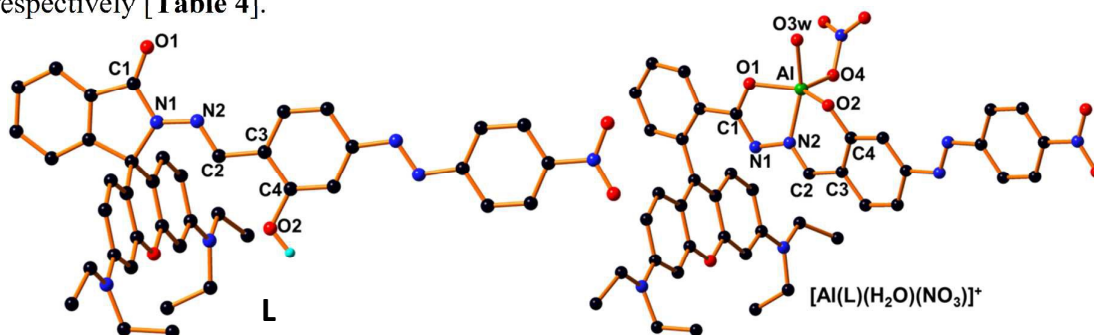


Fig. 10: DFT/B₃LYP optimized geometry of **L** as well as complex [Al(L)(H₂O)(NO₃)]⁺.

Table 1: Selected optimized geometrical parameters for [Al(L)(H₂O)(NO₃)]⁺ (**1**) in the ground state calculated at B₃LYP Levels.

Bond Lengths (Å)			
Al-O1	1.872	Al-O3w	1.919
Al-N2	1.968	Al-O4	1.879
Al-O2	1.795		
Bond Angles (°)			
O1-Al-N2	80.387	O1-Al-O3w	84.931
N2-Al-O2	90.992	O4-Al-O3w	98.613
O2-Al-O3w	92.704	O4-Al-O1	102.170
N2-Al-O3w	156.675	O4-Al-O2	107.929
O2-Al-O1	149.814	O4-Al-N2	102.122

Table 2: Change in bond lengths for **1** compared to free **L** in the ground state calculated at B₃LYP Levels

Bond Lengths (Å)		
	Free ligand (L)	[Al(L)(H ₂ O)(NO ₃)] ⁺
N1–C1	1.418	1.323
O1–C1	1.238	1.348
N1–N2	1.335	1.414
N2–C2	1.288	1.313
O2–C4	1.392	1.350

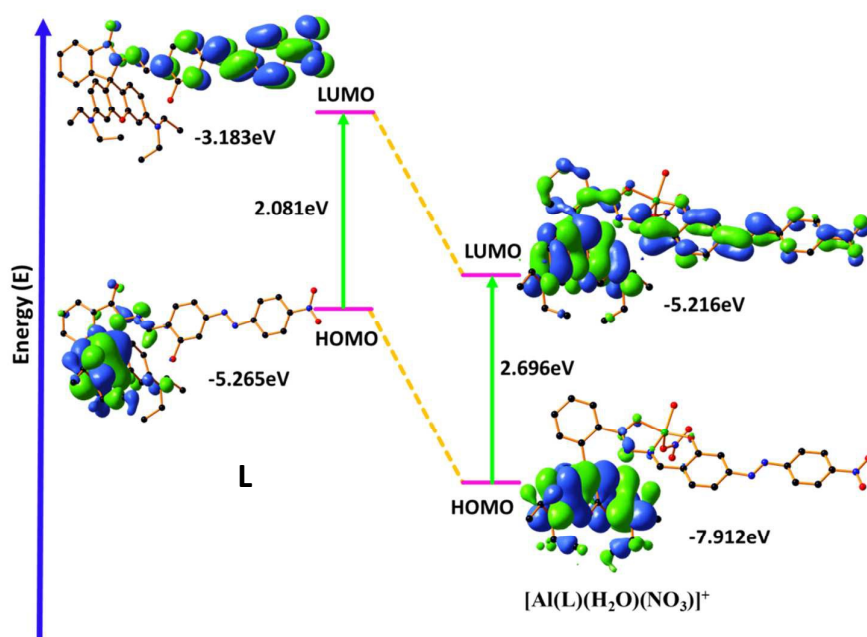


Fig. 11: Frontier molecular orbital of complex as well as **L** optimized.

Table 3: Selected Parameters for the vertical excitation (UV-Vis absorptions) of **L**; electronic excitation energies (eV) and oscillator strengths (*f*), configurations of the low-lying excited states of **L**; calculation of the S₀→S₁ energy gaps based on optimized ground-state geometries (UV-Vis absorption) (methanol used as solvent).

Electronic transition	Composition	Excitation energy	Oscillator strength (f)	CI	λ_{exp} (nm)
$S_0 \rightarrow S_{14}$	HOMO - 3 \rightarrow LUMO + 1	3.1905 eV (388nm)	0.1089	0.37097	385
	HOMO - 2 \rightarrow LUMO + 1			0.11323	
	HOMO - 1 \rightarrow LUMO + 2			0.41736	

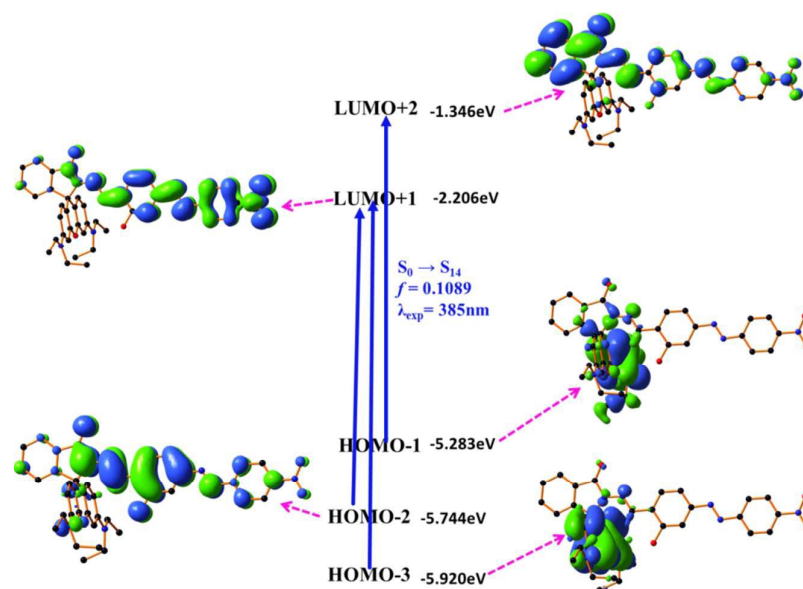


Fig. 12: Frontier molecular orbitals involved in the UV-Vis absorption of **L**.

Table 4: Main calculated optical transition for the complex **1** with composition in terms of molecular orbital contribution of the transition, vertical excitation energies, and oscillator strength in methanol.

Electronic transition	Composition	Excitation energy	Oscillator strength (f)	CI	λ_{exp} (nm)
$S_0 \rightarrow S_2$	HOMO - 2 \rightarrow LUMO	2.4163 eV (545 nm)	0.2106	0.15464	553
	HOMO \rightarrow LUMO			0.50524	
$S_0 \rightarrow S_3$	HOMO - 2 \rightarrow LUMO	2.5413 eV (513 nm)	0.6006	0.17444	514
	HOMO - 1 \rightarrow LUMO			0.67454	
$S_0 \rightarrow S_{11}$	HOMO - 5 \rightarrow LUMO	3.1073 eV (399 nm)	0.0505	0.67380	400
	HOMO - 2 \rightarrow LUMO + 1			0.13700	

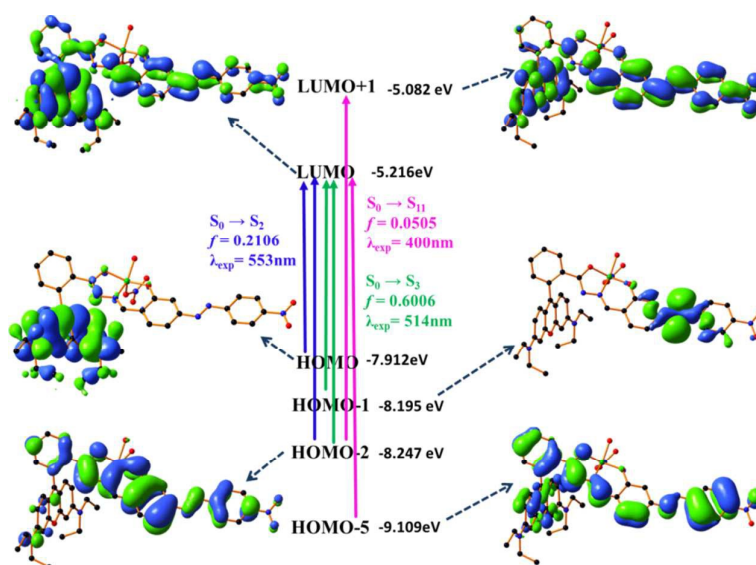


Fig. 13: Frontier molecular orbitals involved in the UV-Vis absorption of complex 1.

Fluorescence lifetime measurements

The sample was excited using a laser diode at 450 nm and the signals were collected at the magic angle of 54.7° to eliminate any considerable contribution from fluorescence anisotropy decay.⁵² The typical time resolution of our experimental setup is ~ 100 ps. The decays were deconvoluted using DAS-6 decay analysis software. The acceptability of the fits was judged by χ^2 criteria and visual inspection of the residuals of the fitted function to the data. Mean (average) fluorescence lifetimes were calculated using the following equation.^{60,61}

$$\tau_{av} = \frac{\sum \alpha_i \tau_i^2}{\sum \alpha_i \tau_i}$$

in which α_i is the pre-exponential factor corresponding to the i^{th} decay time constant, τ_i .

To gain an insight into the sensing mechanism we performed TCSPC measurements of **L** and **L-Al³⁺** ensemble using a 450 nm nano-LED as the excitation source. The decay behaviour of the bare fluorophore, its metal complex is found to be complicated and is best fitted to triexponential functions. Bare **L** showed three components having lifetimes 1.46, 5.21 and 0.12 ns respectively. The populations of the same were 0.08, 0.03 and 0.89 % respectively. The average lifetime, calculated using standard methods was calculated to be 1.20 ns. Upon addition of **Al³⁺**, three components were obtained having lifetimes 0.95, 0.07 and 4.13 ns respectively, having populations of 0.18, 0.79 and 0.03 % respectively (**Table 5**). The average lifetime was calculated to be 3.00 ns. Thus, **L-Al³⁺** ensemble underwent an increment in lifetime compared to free **L**. The results are indicative of inhibited PET

mechanism and CHEF mechanism where freezing of non-radiative pathways leads to an increment in the excited state lifetime.

Table 5: Fluorescence lifetimes of **L** and **L-Al³⁺** complex MeOH solvent

MeOH	τ_1 (ns)	τ_2 (ns)	τ_3 (ns)	α_1	α_2	α_3	χ^2	τ_{av}
L	1.46	5.21	0.12	0.08	0.03	0.89	1.12	1.20
L-Al³⁺	0.95	0.07	4.13	0.18	0.79	0.03	1.08	3.00

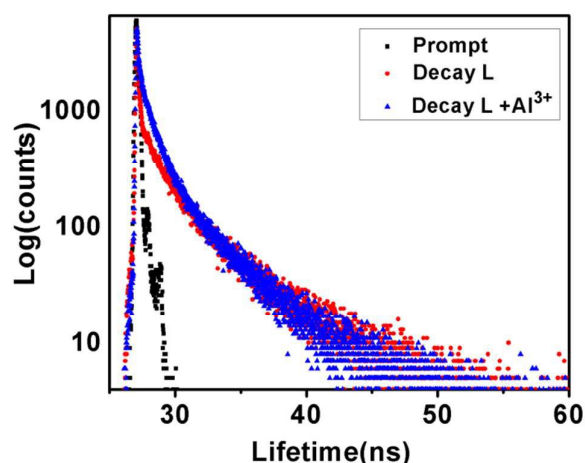


Fig. 14: TCSPC measurements of **L** and **L-Al³⁺** ($\lambda_{ex} = 450$ nm)

Conclusion

In summary, we developed a new sensor **L**, which displays a significant change of both colorimetric and fluorometric response upon the Al^{3+} binding. Upon addition of Al^{3+} chemosensor changes its colour from colour less to pink due to the both PET and CHEF process which can be observed in naked eye. Fluorometric measurements of Al^{3+} with receptor high binding constant, nonlinear-least squares fitting of titration profiles and nanomolar level detection limit all supports the 1:1 binding complex of metal with chemosensor. We believe that excellent selectivity and reversibility of this chemosensor to Al^{3+} helps us to consider it as a practical probe for detection of Al^{3+} in naked eye.

Conflicts of interest

There are no conflicts of interest to declare.

Acknowledgements

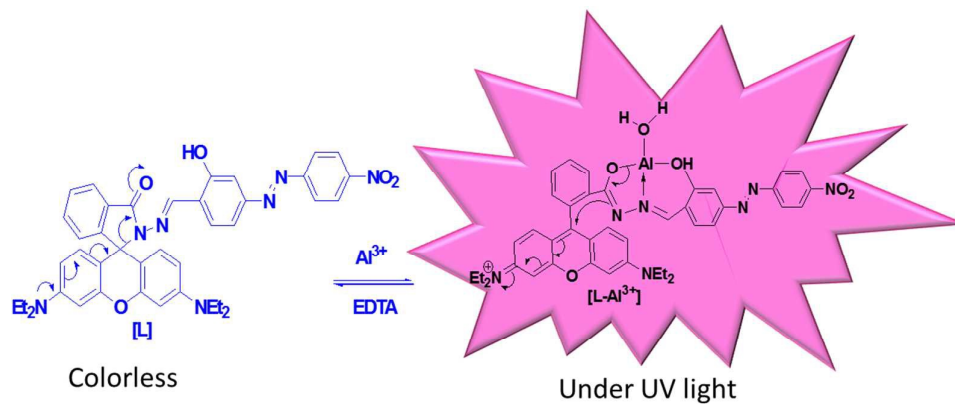
S. Dey is grateful to the University Grants Commission, New Delhi, India, for financial support by sanctioning a minor research project (Sanction letter No. PSW-155/14-15(ERO) ID No. WV6- 027, S. No. 223832 dated 03-02-2015). A. Dhara acknowledges the financial support provided by University Grants Commission, India (Award letter No. F.4-2/2006(BSR)/CH/14-15/0163; dated May, 2015) through the Dr. D. S. Kothari Post-Doctoral Fellowship (DSKPDF). SM acknowledges the contribution of Dr. Milan Kr. Barman, NISER, Bhubaneswar and Nirmalya Acharya, Mahishadal Raj College for their critical scientific suggestions.

References

- 1 G. Berthon, *Coord. Chem. Rev.*, 1996, **149**, 241–280.
- 2 T. P. Flaten, *Brain Res. Bull.*, 2001, **55**, 187–196.
- 3 P. Nayak, *Environ. Res.*, 2002, **89**, 101–115.
- 4 M. G. Soni, S. M. White, W. G. Flamm and G. A. Burdock, *Regul. Toxicol. Pharmacol.*, 2001, **33**, 66–79.
- 5 E. Gauthier, I. Fortier, F. Courchesne, P. Pepin, J. Mortimer and D. Gauvreau, *Environ. Res.*, 2000, **84**, 234–246.
- 6 S. Kim, J. Y. Noh, K. Y. Kim, J. H. Kim, H. K. Kang, S. W. Nam, S. H. Kim, S. Park, C. Kim and J. Kim, *Inorg. Chem.*, 2012, **51**, 3597–3602.
- 7 Y. Y. Guo, L. Z. Yang, J. X. Ru, X. Yao, J. Wu, W. Dou, W. W. Qin, G. L. Zhang, X. L. Tang and W. S. Liu, *Dye. Pigment.*, 2013, **99**, 693–698.
- 8 S. Sharma, M. S. Hundal, A. Walia, V. Vanita and G. Hundal, *Org. Biomol. Chem.*, 2014, **12**, 4445–53.
- 9 Y. G. Zhang, Z. H. Shi, L. Z. Yang, X. L. Tang, Y. Q. An, Z. H. Ju and W. S. Liu, *Inorg. Chem. Commun.*, 2014, **39**, 86–89.
- 10 V. Kumar, A. Kumar, U. Diwan, Shweta, Ramesh, S. K. Srivastava and K. K. Upadhyay, *Sensors Actuators, B Chem.*, 2015, **207**, 650–657.
- 11 L. He, C. Liu and J. H. Xin, *Sensors Actuators, B Chem.*, 2015, **213**, 181–187.
- 12 M. Dong, Y. M. Dong, T. H. Ma, Y. W. Wang and Y. Peng, *Inorganica Chim. Acta*, 2012, **381**, 137–142.
- 13 X. Xie and Y. Qin, *Sensors Actuators, B Chem.*, 2011, **156**, 213–217.
- 14 B. Jisha, M. R. Resmi, R. J. Maya and R. L. Varma, *Tetrahedron Lett.*, 2013, **54**, 4232–4236.
- 15 Y. Wang, L. J. Hou, Y. B. Wu, L. L. Shi, Z. Shang and W. J. Jin, *J. Photochem. Photobiol. A Chem.*, 2014, **281**, 40–46.

- 16 J. C. Qin and Z. Y. Yang, *J. Photochem. Photobiol. A Chem.*, 2015, **303–304**, 99–104.
- 17 C. J. Liu, Z. Y. Yang, L. Fan, X. L. Jin, J. M. An, X. Y. Cheng and B. D. Wang, *J. Lumin.*, 2015, **158**, 172–175.
- 18 O. Alici and S. Erdemir, *Sensors Actuators, B Chem.*, 2015, **208**, 159–163.
- 19 E. Oliveira, H. M. Santos, J. L. Capelo and C. Lodeiro, *Inorganica Chim. Acta*, 2012, **381**, 203–211.
- 20 L. Yuan, W. Lin, B. Chen and Y. Xie, *Org. Lett.*, 2012, **14**, 432–5.
- 21 Y. Liu, X. Lv, Y. Zhao, M. Chen, J. Liu, P. Wang and W. Guo, *Dye. Pigment.*, 2012, **92**, 909–915.
- 22 V. Bhalla, R. Tejpal and M. Kumar, *Sensors Actuators B. Chem.*, 2010, **151**, 180–185.
- 23 L. Huang, X. Wang, G. Xie, P. Xi, Z. Li, M. Xu, Y. Wu, D. Bai and Z. Zeng, , DOI:10.1039/c0dt00606h.
- 24 C. Wang and K. M. C. Wong, *Inorg. Chem.*, 2013, **52**, 13432–13441.
- 25 S. H. Kim, H. S. Choi, J. Kim, S. J. Lee, D. T. Quango and J. S. Kim, *Org. Lett.*, 2010, **12**, 560–563.
- 26 A. Dhara, A. Jana, N. Guchhait, P. Ghosh and S. K. Kar, *New J. Chem.*, 2014, **38**, 1627.
- 27 B. Sen, M. Mukherjee, S. Banerjee, S. Pal and P. Chattopadhyay, *Dalt. Trans.*, 2015, **44**, 8708–8717.
- 28 A. Sahana, A. Banerjee, S. Lohar, B. Sarkar, S. K. Mukhopadhyay and D. Das, *Inorg. Chem.*, 2013, **52**, 3627–3633.
- 29 A. Jana, P. K. Sukul, S. K. Mandal, S. Konar, S. Ray, K. Das, J. a Golen, A. L. Rheingold, S. Mondal, T. K. Mondal, A. R. Khuda-Bukhsh and S. K. Kar, *Analyst*, 2014, **139**, 495–504.
- 30 C. Lee, W. Yang and R. Parr, *Phys. Rev. B*, 1988, **37**, 785–789.
- 31 V. Barone and M. Cossi, *J. Phys. Chem. A*, 2001, **102**, 1995–2001.
- 32 M. Cossi and V. Barone, *J. Chem. Phys.*, 2001, **115**, 4708–4717.
- 33 M. Cossi, N. Rega, G. Scalmani and V. Barone, *J. Comput. Chem.*, 2003, **24**, 669–681.
- 34 A. D. Becke, *J. Chem. Phys.*, 1993, **98**, 5648–5652.
- 35 M. E. Casida, C. Jamorski, K. C. Casida and D. R. Salahub, *J. Chem. Phys.*, 1998, **108**, 4439–4449.
- 36 R. E. Stratmann, G. E. Scuseria and M. J. Frisch, *J. Chem. Phys.*, 1998, **109**, 8218–8224.
- 37 R. Bauernschmitt and R. Ahlrichs, 1996, **256**, 454–464.
- 38 T. Liu, H.-X. Zhang, X. Shu and B.-H. Xia, *Dalt. Trans.*, 2007, 1922.
- 39 C. H. Oh, 2005, **5**, 8809–8818.

- 40 X. Zhou, A.-M. Ren and J.-K. Feng, *J. Organomet. Chem.*, 2005, **690**, 338–347.
- 41 A. Albertino, C. Garino, S. Ghiani, R. Gobetto, C. Nervi, L. Salassa, E. Rosenberg, A. Sharmin, G. Viscardi, R. Buscaino, G. Croce and M. Milanese, *J. Organomet. Chem.*, 2007, **692**, 1377–1391.
- 42 D. G. Truhlar, *J. Comput. Chem.*, 2009, **28**, 73–86.
- 43 B. G. Rao, Y. Usha, P. S. Reddy and P. V. Rao, *Int. J. Innov. Reserch Dev.*, 2013, **2**, 39–43.
- 44 M. S. Bashandy, F. A. Mohamed, M. M. El-Molla, M. B. Sheier and A. H. Bedair, *Open J. Med. Chem.*, 2016, **6**, 18–35.
- 45 Y. Xiang, A. Tong, P. Jin and Y. Ju, *Org. Lett.*, 2006, **8**, 2863–2866.
- 46 H. A. Benesi and J. H. Hildebrand, *J. Am. Chem. Soc.*, 1949, **71**, 2703–2707.
- 47 R. Tang, K. Lei, K. Chen, H. Zhao and J. Chen, *J. Fluoresc.*, 2011, **21**, 141–148.
- 48 A. Jana, B. Das, S. K. Mandal, S. Mabhai, A. R. Khuda-Bukhsh and S. Dey, *New J. Chem.*, 2016, **40**, 5976–5984.
- 49 J. Cheng, X. Zhou and H. Xiang, *Analyst*, 2015, **140**, 7082–7115.
- 50 A. Dhara, A. Jana, N. Guchhait, P. Ghosh and S. K. Kar, *New J. Chem. New J. Chem*, 2014, **38**, 1627–1634.
- 51 D. Maity and T. Govindaraju, *Inorg. Chem.*, 2010, **49**, 7229–7231.
- 52 J. R. Lakowicz, *Plenum, New York*.
- 53 D. Udhayakumari, S. Velmathi, Y. M. Sung and S. P. Wu, *Sensors Actuators, B Chem.*, 2014, **198**, 285–293.
- 54 T. Mistri, R. Alam, M. Dolai, S. Kumar Mandal, P. Guha, A. Rahman Khuda-Bukhsh and M. Ali, *Eur. J. Inorg. Chem.*, 2013, 5854–5861.
- 55 P. Mahato, S. Saha, E. Suresh, R. Di Liddo, P. P. Parnigotto, M. T. Conconi, M. K. Kesharwani, B. Ganguly and A. Das, *Inorg. Chem.*, 2012, **51**, 1769–77.
- 56 K. Ghosh, T. Sarkar and A. Samadder, *Org. Biomol. Chem.*, 2012, **10**, 3236.
- 57 A. R. K.-B. and P. C. Buddhadeb Sen, Siddhartha Pal, Somenath Lohar, Manjira Mukherjee, Sushil Kumar Mandal, *RSC Adv.*, 2014, 21471–21478.
- 58 V. K. Gupta, N. Mergu, L. K. Kumawat and A. K. Singh, *Talanta*, 2015, **144**, 80–89.
- 59 S. Mabhai, A. Jana and S. Dey, *J. Indian Chem. Soc.*, 2015, **92**, 1–10.
- 60 S. Banthia and A. Samanta, *J. Phys. Chem. B*, 2006, **110**, 6437–40.
- 61 B. Ramachandram, G. Saroja, B. Sankaran and A. Samanta, *J. Phys. Chem. B*, 2000, **104**, 11824–11832.

Graphical Abstract:

Both rhodamine and azobenzene moiety have been conjugated to prepare a novel chemosensor for the detection of Al³⁺ through CHEF-PET and spirolactam ring opening mechanism.